

# Discovery of Correlated Behavior Between the HXR and the Radio Bands in Cygnus X-3

M. L. McCollough, C. R. Robinson, S. N. Zhang

Universities Space Research Association, Huntsville, AL 35805, U.S.A.

B. A. Harmon

NASA/Marshall Space Flight Center, Huntsville, AL 35812, U.S.A.

R. M. Hjellming

National Radio Astronomy Observatory, Socorro, NM 87801, U.S.A.

E. B. Waltman, R. S. Foster

Naval Research Laboratory, Washington, DC 20375, U.S.A.

F. D. Ghigo

National Radio Astronomy Observatory, Green Bank, WV 24944, U.S.A.

M. S. Briggs, G. N. Pendleton

Department of Physics, University of Alabama in Huntsville, Huntsville, AL 35899, U.S.A.

and

K. J. Johnston

United States Naval Observatory, Washington, DC 20392, U.S.A.

Received \_\_\_\_\_; accepted \_\_\_\_\_

To be submitted to Ap.J. Letters

## ABSTRACT

Using CGRO/BATSE hard X-ray (HXR) data and GHz radio monitoring data from the Green Bank Interferometer (GBI), we have performed a long term study ( $\sim 1800$  days) of the unusual X-ray binary Cyg X-3 resulting in the discovery of a remarkable relationship between these two wavelength bands. We find that, during quiescent radio states, the radio flux is strongly anticorrelated with the intensity of the HXR emission. The relationship switches to a correlation with the onset of major radio flaring activity. During major radio flaring activity the HXR drops to a very low intensity during quenching in the radio and recovers during the radio flare. Injection of plasma into the radio jets of Cyg X-3 occurs during changes in the HXR emission and suggests that disk-related and jet-related components are responsible for the high energy emission.

*Subject headings:* X-ray: stars; radio continuum: stars; Stars: individual: Cygnus X-3

## 1. INTRODUCTION

Cyg X-3 is a very unusual X-ray binary (see Bonnet-Bidaud & Chardin 1988 for a review) which does not fit well into any of the established classes of X-ray binaries. A 4.8 hour modulation, thought to be the orbital period of the binary, is observed at X-ray (Brinkmann et al. 1972, Parsignault et al. 1972) and infrared (Becklin 1972, Mason et al. 1986) wavelengths. The 4.8 hour orbital period is typical of a low mass X-ray binary, but infrared observations suggest that the mass donating companion is a high mass Wolf-Rayet star (van Kerkwijk et al. 1992). Due to the distance ( $> 8.4$  kpc; see Bonnet-Bidaud & Chardin 1988), and its location in the Galactic plane, no optical counterpart has been found.

Cyg X-3 is also a strong source of radio emission with three types of behavior: (a) quiescence, (b) major flaring with quenching (very low radio fluxes), and (c) minor radio flaring with partial quenching (see Waltman et al. 1994, 1995, 1996). During the major radio outbursts there is strong evidence of jet-like structures moving away from Cyg X-3 at a velocity of either  $\sim 0.3c$  or  $\sim 0.6c$ , depending upon whether the jets are one-sided or double-sided ( Molnar et al. 1988, Schalinski et al. 1995). Recent VLBA images after a large Cyg X-3 flare showed one-sided ejection with  $v \gtrsim 0.8c$  (Mioduszewski et al. 1998).

The soft X-ray emission (below 20 keV) from Cyg X-3 has been observed to undergo high and low states in which the various spectral components change with no apparent correlation with other properties (White et al. 1995). From Ginga observations (Watanabe et al. 1994), it was found that the giant radio flares occur only when the soft X-ray flux is high. Hard X-ray (HXR) observations (above  $\sim 50$  keV), prior to 1991, found the HXR emission to vary by less than 20% (White & Holt 1982, Hermsen et al. 1992). Recent Compton Gamma-Ray Observatory (CGRO) observations of Cyg X-3 made using OSSE have shown HXR emission to be variable by a factor of 3 (Matz et al. 1994).

In this letter, we report results obtained from the nearly continuous monitoring of Cyg X-3 for a period of almost 5 years in both the HXR (CGRO/BATSE) and the radio wavelength bands. Cyg X-3 has been monitored in the HXR and radio as part of a study to understand the high-energy properties of binary X-ray sources and how they relate to the production of jets.

## 2. HARD X-RAY OBSERVATIONS

The BATSE experiment onboard CGRO (Fishman et al. 1989) was used to monitor the HXR emission from Cyg X-3. The BATSE Large Area Detectors (LADs) can monitor the whole sky almost continuously in the energy range of 20 keV–2 MeV with a typical daily  $3\sigma$  sensitivity of about 100 mCrab.

To produce the Cyg X-3 light curve, single step occultation data were obtained using a standard Earth occultation analysis technique for monitoring HXR sources (Harmon et al. 1992). Interference from known bright sources (such as Cyg X-1) and single steps with large deviations from the median flux measurement (the result of the HXR flaring behavior of Cyg X-1) were removed. The single occultation step data were then fit with a power law with a fixed photon spectral index of  $-3.0$  to determine a flux in the 20–100 keV band. The spectral index was chosen based on spectral fitting of the BATSE data during periods of high levels of emission and is consistent with the index found by Matz et al. 1994 from OSSE observations. Varying the spectral index, for an acceptable range of spectral indices, results in a 10–15 % variation in the measured flux.

A Lomb-Scargle periodogram (Lomb 1976, Scargle 1982) was created for the single step occultation data to search for periodicities in the data. The known 4.8 hour period of Cyg X-3 was detected in the BATSE data set at a very high significance (Robinson et al. 1997),

with no additional periodicities being found in the data. Sums of single step occultation data of  $\geq 2$  day duration were found to uniformly sample all phases of the 4.8 hour period.

### 2.1. Hard X-Ray Light Curve

Fig. 1 shows a history of the 20–100 keV HXR emission from Cyg X-3. The BATSE data were binned with each point containing 40 occultation steps, with each occultation step having an integration time of 110 seconds. This corresponds to about three days of observations per data point. Cyg X-3 ranges from less than BATSE’s three day detection limit of  $\sim 40$  mCrab to intensities at least 7 times brighter. The two most distinctive features in the HXR light curves are (a) extended periods of high HXR flux (0.04 – 0.08 ph cm $^{-2}$  sec $^{-1}$ ) and (b) low flux periods where the flux level drops below the detection limit of BATSE.

## 3. RADIO OBSERVATIONS

Cyg X-3 was observed on a daily basis as part of the Naval Research Laboratory Green Bank Interferometer (GBI) Monitoring Program. The GBI consists of two 25.9 m diameter antennas separated by a 2.4 km baseline. The antennas each observe simultaneously at 2.25 and 8.3 GHz with 35 MHz of total bandwidth at each frequency. The observing and data reduction techniques are described in Fiedler et al. 1987, Waltman et al. 1994, and Waltman et al. 1995. The average integration time for individual scans is approximately 10 minutes with up to 12 scans made on the source per day. Typical errors ( $1\sigma$ ) in the GBI data set are flux density dependent : 4 mJy (2 GHz) or 6 mJy (8 GHz) for fluxes less than 100 mJy; 15 mJy (2 GHz) or 50 mJy (8 GHz) for fluxes  $\sim 1$  Jy. In Fig. 1 the 2.25 GHz radio flux densities are shown overlaid on a log scale for the same time period as the HXR

measurements.

#### 4. THE HARD X-RAY – RADIO RELATIONSHIPS

What is striking to the eye is an overall anticorrelation between the radio and the HXR emission. At the times when the radio has become quiescent the HXR increases and goes into a state of high emission. With the occurrence of radio flares the HXR emission drops and during the major flaring activity the behavior of the HXR and radio changes to a correlation (see Fig. 2).

To test fully the existence of these (anti)correlations we calculated correlation coefficients ( $r_s$ ) and probability functions of the Spearman rank-order. To assure that each pair of points is statistically independent, rejection of some fraction of the data to eliminate any internal correlation is necessary.<sup>1</sup>

For each of the two time series we divided the data into two sets of observations consisting of alternating measurements from the original time series. These series were tested and if an internal correlation was found, we then rejected half of the data points and repeated the procedure with the remaining data. We continued this process until at least one of the two different time series showed no internal correlation, then tested the matching data points in the time series of the two wavelength bands for a correlation. In all cases we consider a correlation to exist if the probability of no correlation was  $10^{-3}$  or less.

Table 1 shows the results of correlation testing using 3 day averages of the data for

---

<sup>1</sup>Care must be taken because if the time series contain internal correlations then a correlation test between the two time series can result in either a false or enhanced correlation (Walther 1997).

different sets of the data. For each type of activity is given (a) the Spearman correlation coefficient, (b) probability of no correlation, (c) initial size of the data set, (d) size of the data set after data rejection, and (e) the wavelength band (R: Radio, X: HXR, B: Both) in which there is no internal correlation.

*Entire Data Sets:* During times of high HXR flux the radio data show less variability and as flaring occurs, the HXR starts to drop. One can define a variability index by taking the standard deviation ( $\sigma$ ) in the radio data, over the time averaged interval, and dividing it by the mean value of the radio flux ( $\langle S \rangle$ ) for the time averaged interval. Table 1 and Fig. 3 shows the existence of a strong anticorrelation between the HXR flux and the variability index of the radio flux.

*Quiescence Radio Activity:* For the periods of quiescent radio emission in our data sets we see that there is a very strong anticorrelation between the HXR and the radio fluxes.

*Major Flaring Activity:* For major flaring activity one can see there exists a strong correlation between the HXR and the radio fluxes (see Fig. 2). OSSE observations made during the first major radio flare activity period showed a factor of 3 drop in the HXR as the radio became quenched prior to a major flare and later observations showed a higher flux level as Cyg X-3 returned to quiescence (Matz et al. 1994) in agreement with the BATSE data.

*Minor Flaring Activity:* During the minor flaring there was no significant correlation found between the HXR and radio fluxes.

Fig. 4 is a radio versus HXR flux plot for the radio quiescent periods and the major radio flare activity. In this plot we see two branches which describe the correlated behavior which we have found. There is a horizontal branch which describes the quiescent radio state and a vertical branch which describes the major radio flaring. It is of interest to note that

where the two branches overlap one finds the minor radio flaring data points.

## 5. DISCUSSION

For the first time, we report correlated HXR and radio emission in Cyg X-3 (see Table 2 for a summary). The high degree of anticorrelation, during radio quiescence, between the wavelength bands indicates that the same high energy particle production mechanism may be responsible for the particles which produce both the radio (synchrotron) and hard X-ray (Compton processes). However the efficiency of inverse-Compton processes (Shu 1991) in cooling the high energy electrons required to produce the synchrotron radio emission make it unlikely the HXR and radio originate from the same emission region. These high energy particles may be the result of either the production of a “hot” corona (White & Holt 1982) or the presence of a low-level jet (Fender et al. 1997), during a period of low mass transfer in the system.

The major radio flaring activity represents a distinct change in the behavior of the system. The quenched radio emission preceding large to medium radio flares clearly corresponds to low HXR states in the BATSE data. Such episodes have been interpreted (Fender et al. 1997), based on the increase in soft X-rays (Kitamoto et al. 1994), as an indication of a large increase in mass flow within an accretion disk prior to a major radio flare. The nature of this radio emission during the preflare episodes is not understood, but possibly both the HXR and radio fluxes are generated in a region (initially optically thick) near the central object. It is apparent that the quenched radio emission and the low HXR state are tied to the formation of the jet.

When a large radio flare occurs, there is a corresponding increase in the HXR flux. As the radio flare decays, the HXR also drops on a similar timescale. The decay in the

HXR may be interrupted by subsequent flares or a transition to a radio quiescent state. The radio flare can be interpreted as a consequence of an ejection event from a bipolar or one-sided jet (Schalinski et al. 1998, Mioduszewski et al. 1998) where the radio flare is due to the growth in solid angle and expansion of the developing jets. The HXR emission is most likely the result of inverse Compton processes, but the site of this emission is less certain. Early observations of the galactic jet sources, GRS 1915+105 (Foster et al. 1996) and GRO J1655-40 (Harmon et al 1995), which showed a correlation between the HXR and radio, gave rise to models in which the HXR emission arose from the jet (Levinson & Blandford 1996). But later observations of these two sources have shown HXR outbursts with which there was no accompanying radio jets (GRO J1655-40; Zhang et al. 1997) or there was an anticorrelation between the radio flare and the HXR flux (GRS 1915+105; Harmon et al. 1997). While there may be uncertainty on the site of the HXR emission it is clear that there is HXR response for all of the major flares (and associated jets) in Cyg X-3.

During minor radio flaring periods there occur smaller “mini-flares” and a drop in the overall HXR flux which is reflected in the anti-correlation between HXR flux and the radio variability index. It is possible that conditions exist here similar to those present during the major radio outbursts, although the relatively low intensity in HXRs makes it difficult to check if the faster variability seen in the radio is also reflected at the same timescales in HXRs.

Kitamoto et al. 1994 have suggested that the X-ray and radio activity are mediated by the dense wind from the companion star. In the quiescent radio state, the wind density is predicted to be low. Changes in the wind may determine whether the source changes from a radio quiescence/HXR high state to radio flaring/HXR low state.

## ACKNOWLEDGMENTS

Basic research in radio astronomy at the Naval Research Laboratory is supported by the Office of Naval Research. The Green Bank Interferometer was operated by the National Radio Astronomy Observatory under contract to the U.S. Naval Observatory during the time period of these observations. The National Radio Astronomy Observatory is operated by Associated Universities, Inc. under a Cooperative Agreement with the National Science Foundation.

## REFERENCES

Becklin, E.E., et al. 1972, *Nature Phys. Sci.*, 239, 134

Bonnet-Bidaud, J.M. & Chardin, G. 1988, *Phys. Rep.*, 170, 326

Brinkmann, A. et al. 1972, *IAU Circ.*, 2446

Fender, R.P., et al. 1997, *MNRAS*, 288, 849

Fiedler, R.L., et al. 1987, *ApJS*, 65, 319

Fishman, G.J., et al. 1989, in *Proc. Gamma-Ray Observatory Science Workshop*, ed. W. N. Johnson (Greenbelt: Goddard Space Flight Center), 39

Foster, R.S., et al. 1996, *ApJ*, 467, L81

Geldzahler, B.J., et al. 1983, *ApJ*, 273, L65

Harmon, B.A et al. 1992, in *The Compton Observatory Workshop*, NASA CP 3137, ed. C.R. Shrader, N. Gehrels, & B. Dennis, 69

Harmon, B.A et al. 1995, *Nature*, 374, 703

Harmon, B.A et al. 1997, *ApJ*, 477, L85

Hermsen, W., et al. 1987, *A&A*, 175, 141

Kitamoto, S. et al 1994, *A&A*, 281, L85

Lomb, N.R. 1976, *Ap&SS*, 39, 447

Levinson, A. & Blandford, R. 1996, *ApJ*, 456, L29

Mason, K.O., et al. 1986, *ApJ*, 309, 700

Matz, S.M., et al. 1994, in The Evolution of X-Ray Binaries ed. S.S. Holt and C.S. Day (New York: AIP), p. 263

Mioduszewski, A.J. et al. 1998, Proc. of IAU Colloquium 164, 351

Molnar, L.A., et al. 1988, ApJ, 331, 494

Parsignault, D., et al. 1972, *Nature Phys. Sci.*, 239, 123

Robinson, C.R. et al, 1997, in “Transparent Universe”, ESA, SP-382, 249

Schalinski, C.J. et al, 1995, ApJ, 447, 752

Schalinski, C.J. et al, 1998, A&A, 329, 504

Scargle, J.D., 1982, ApJ, 263, 835

Shu, E.H., et al. 1991, The Physics of Astrophysics (Mill Valley: University Science Books)

van Kerkwijk, M.H., et al. 1992, Nature, 355, 703

Walther, G., 1997, Phys. Rev. Lett., 179, 4522

Waltman, E.B., et al. 1994, AJ, 108, 179

Waltman, E.B., et al. 1995, AJ, 110, 290

Waltman, E.B., et al. 1996, AJ, 112, 2690

Watanabe, H., et al. 1994, ApJ, 433, 350

White, N.E. & Holt, S.S. 1982, ApJ, 257, 318

White, et al 1995, in X-Ray Binaries ed. Lewin,et al (Cambridge University Press), p. 1

Zhang, S.N. et al., 1997, ApJ, 479, 381



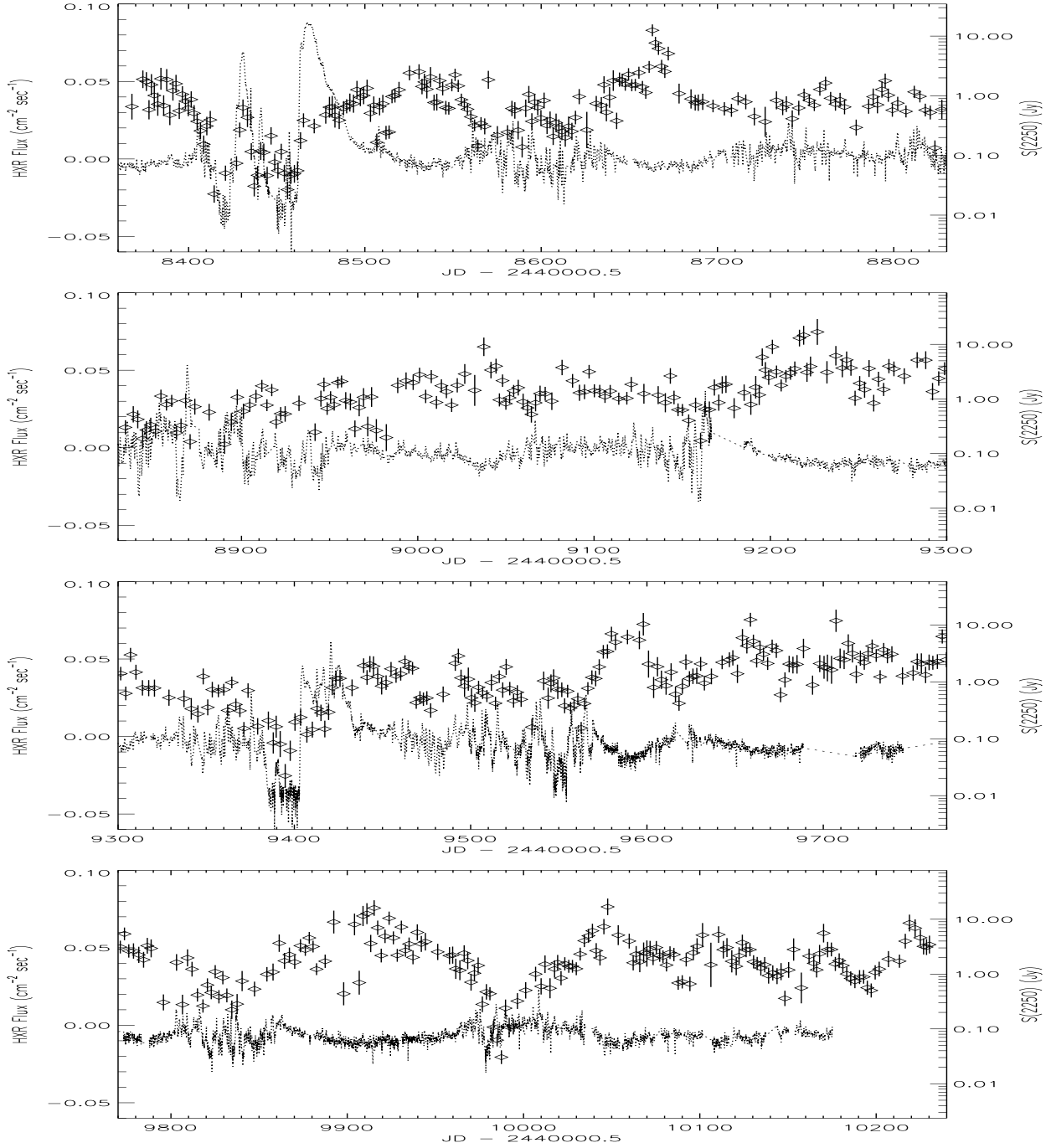


Fig. 1.— A plot of the BATSE 20 - 100 keV flux of Cyg X-3 (diamonds with error bars). Overlayed on a log scale is the 2.25 GHz flux (dotted line) measured by the GBI during the same time interval. The left hand scale ( $\text{ph cm}^{-2}\text{sec}^{-1}$ ) is for the HXR flux and the right hand scale (Jy) is for the 2.25 GHz flux.

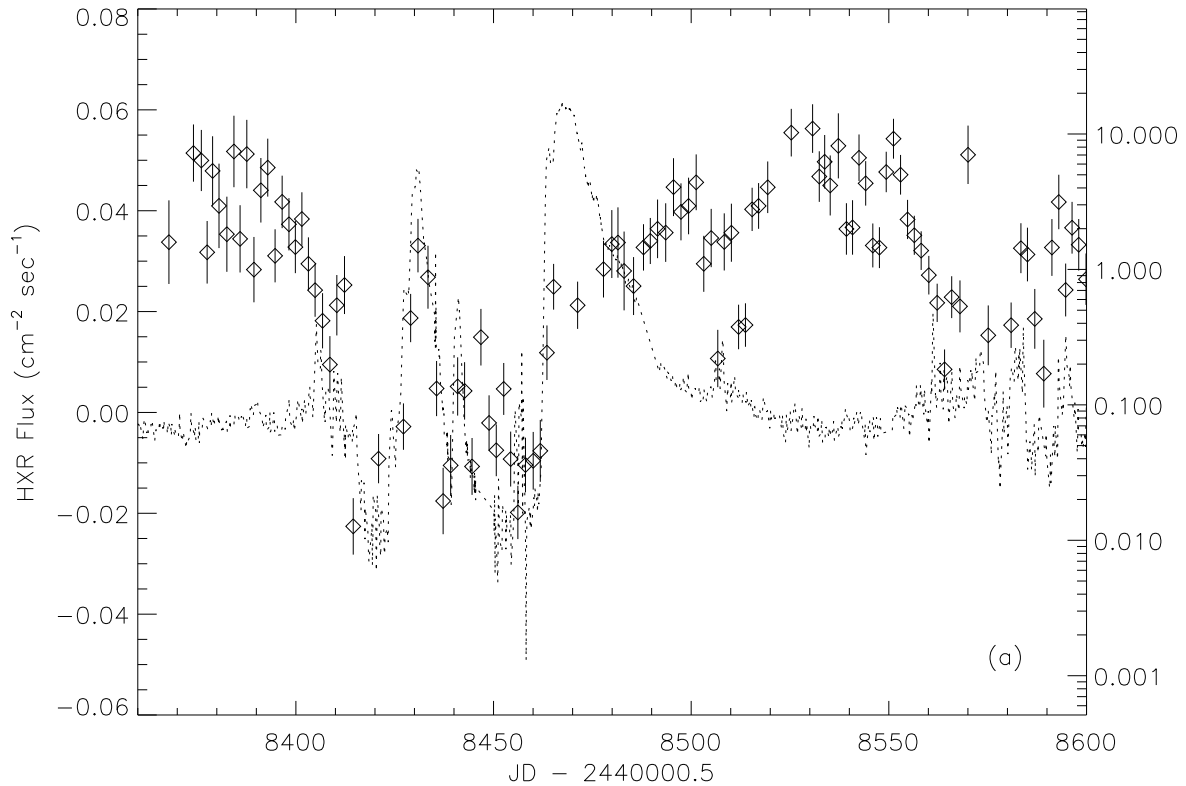


Fig. 2.— HXR flux from Truncated Julian Dates (TJD) 8360 to 8600. Overlaid is the 2.25 GHz flux (dotted line). One can see the transition from a radio quiescent state (anticorrelated with the HXR) into quenched emission and major flares (correlated with HXR) back into a radio quiescent state (anticorrelated with the HXR). One can also see the transition, in the latter radio quiescent state, into a minor flaring state.

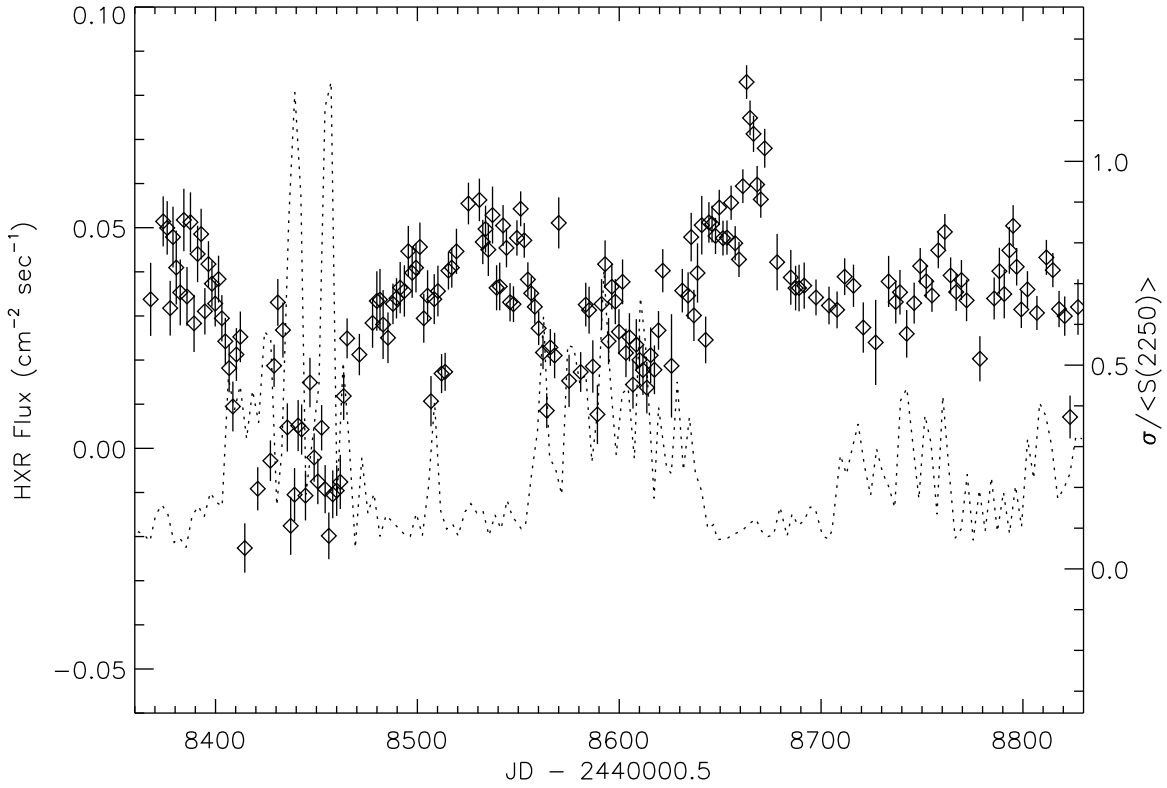


Fig. 3.— HXR flux from TJD 8360 to 8830 (same time range as the top panel of Fig. 1). Overlaid is the variability index of the 2.25 GHz flux (dotted line) for three-day averages. The variability index is defined as  $\sigma / \langle S(2250) \rangle$  where  $\sigma$  is the standard deviation of the data being averaged and  $\langle S(2250) \rangle$  is the mean flux of the radio data being averaged.

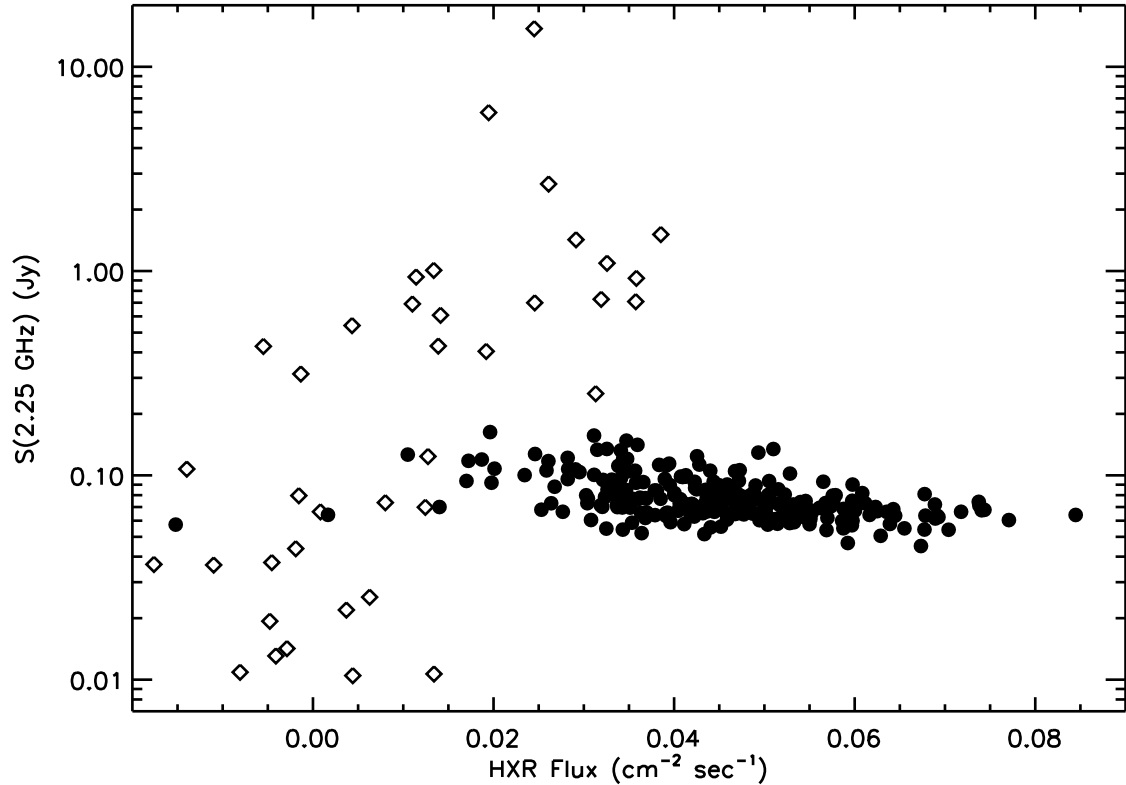


Fig. 4.— This plot contains both the radio quiescent periods (filled circles) and the major flare activity (diamonds) for three day averages. For clarity the minor flaring data (which does not show a correlation) are not plotted, but you would find the majority of minor flaring data points contained within a box defined by 0.0–0.045 ph cm<sup>-2</sup> sec<sup>-1</sup> in the HXR and 0.05–0.30 Jy in the radio. This region corresponds to the area in which radio quiescent periods and the major flare activity overlap one another.

Table 1. Tests of Correlation Between the Data Sets

Spearman					
Source Activity	$r_s$	Prob.	Initial	Final	Band
<b>All Data:</b>					
HXR vs. $\sigma/\langle S(2250) \rangle$	-0.489	$2 \times 10^{-9}$	546	136	R
HXR vs. $\sigma/\langle S(8300) \rangle$	-0.405	$1 \times 10^{-6}$	546	136	R
<b>Quiescence:</b>					
HXR vs. 2.25 GHz	-0.477	$1 \times 10^{-8}$	254	127	X
HXR vs. 8.3 GHz	-0.491	$4 \times 10^{-9}$	254	127	X
<b>Flaring:</b>					
HXR vs. 2.25 GHz (Major)	0.738	$5 \times 10^{-8}$	40	40	B
HXR vs. 8.3 GHz (Major)	0.663	$3 \times 10^{-6}$	40	40	B
HXR vs. 2.25 GHz (Minor)	0.168	$9 \times 10^{-3}$	243	243	R
HXR vs. 8.3 GHz (Minor)	0.190	$4 \times 10^{-2}$	243	121	B

Table 2. Summary of HXR - Radio Relationship

Radio Activity	Relationship	Time Periods (TJD)
<b>All</b>	There exists a anticorrelation between HXR and the variability in the radio.	8361–10175
<b>Quiescence</b>	The HXR and radio show a strong anticorrelation. It is during this state that the HXR reaches its highest levels.	8361–8400, 8500–8557, 8635–8705, 8960–9050, 9170–9330, 9570–9610, 9630–9800, 9860–9975, 10038–10175
<b>Major Radio Flaring</b>	The HXR and radio correlate with the HXR vanishing during quenching and recovering during the major flare.	8415–8500, 8860–8876, 9385–9432
<b>Minor Radio Flaring</b>	The HXR and radio show no correlation for this activity.	8557–8635, 8705–8860, 8876–8960, 9050–9170, 9330–9385, 9432–9570, 9610–9630, 9800–9860, 9975–10038